Bidirectional transport model of morphogen gradient formation via cytonemes

Paul C. Bressloff and Hyunjoong Kim

Department of Mathematics, University of Utah 155 South 1400 East, Salt Lake City, UT 84112

E-mail: `bressloff@math.utah.edu, hkim@math.utah.edu`

Abstract. Morphogen protein gradients play an important role in the spatial regulation of patterning during embryonic development. The most commonly accepted mechanism for gradient formation is diffusion from a source combined with degradation. Recently, there has been growing interest in an alternative mechanism, which is based on the direct delivery of morphogens along thin, actin-rich cellular extensions known as cytonemes. In this paper, we develop a bidirectional motor transport model for the flux of morphogens along cytonemes, linking a source cell to a one-dimensional array of target cells. By solving the steady-state transport equations, we show how a morphogen gradient can be established, and explore how the mean velocity of the motors affects properties of the morphogen gradient such as accumulation time and robustness. In particular, our analysis suggests that in order to achieve robustness with respect to changes in the rate of synthesis of morphogen, the mean velocity has to be negative, that is, retrograde flow or treadmilling dominates. Thus the potential targeting precision of cytonemes comes at an energy cost. We then study the effects of non-uniformly allocating morphogens to the various cytonemes projecting from a source cell. This competition for resources provides a potential regulatory control mechanism not available in diffusion-based models.

Key Words: cytonemes, morphogenesis, protein gradients, robustness, bidirectional transport

1. Introduction

It has been known for some time that protein (morphogen) concentration gradients play a crucial role in the spatial regulation of patterning during development [38]. That is, a spatially varying concentration of a morphogen protein drives a corresponding spatial variation in gene expression through some form of concentration thresholding mechanism. For example, in regions where the morphogen concentration exceeds a particular threshold, a specific gene is activated (see Fig. 1a). Hence, a continuously varying morphogen concentration can be converted into a discrete spatial pattern of differentiated gene expression across a cell population. The most common mechanism of morphogen gradient formation is thought to involve a localized source of protein production within the embryo, combined with diffusion away from the source and subsequent degradation [24, 1, 37, 22, 32, 34]. The latter can arise either from degradation within the extracellular domain or by binding to membrane bound receptors and subsequent removal from the diffusing pool by endocytosis (see Fig. 1b). The rates of binding and internalization thus control the effective degradation rate. The bound receptors can also initiate a signaling cascade resulting in the activation or repression of one or more genes. Coupling these two processes then leads to an effective degradation rate that depends on the local morphogen concentration. For example, a morphogen may activate the expression of its cognate receptor, thus increasing the morphogen degradation rate. This results in a faster degradation rate
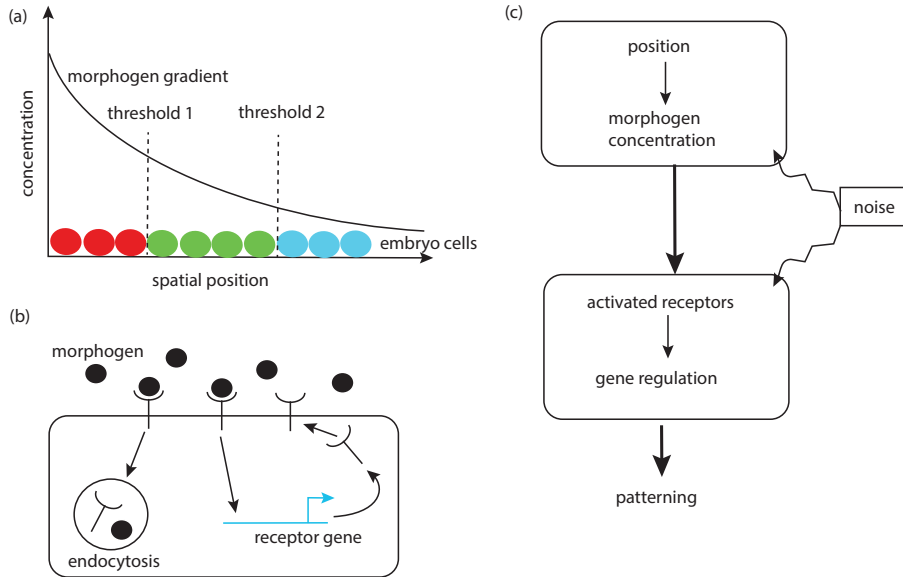
Figure 1. A schematic diagram illustrating how a morphogen gradient acts on embryo cells. (a) Thresholding of the morphogen concentration gradient activate different genes in cells at different locations (indicated by different colors). (b) Morphogens act as signaling molecules that bind to cell receptors and initiate signaling cascades that switch genes on or off. This may include genes responsible for synthesis of the receptors (nonlinear feedback). (c) Morphogenesis has to be robust to noise at different levels, including the morphogen production rate, receptors and genes.

in regions of high morphogen concentration [15]. It is also possible that morphogens are transiently trapped by a cell. Indeed, transient trapping has been suggested as an alternative transport mechanism for morphogens known as transcytosis, whereby repeated rounds of endocytosis and exocytosis results in a dispersion of the molecules within the tissue [21, 9]. In addition to the establishment of morphogen gradients, another important issue concerns possible mechanisms for maintaining the robustness of morphogen-based patterning with respect to changes in environmental conditions such as the morphogen production rate, and stochastic process at the level of receptors and gene circuits that interpret the signal [15, 8, 2, 23, 40, 26, 36], see Fig. 1c. Robustness is related to the problem of morphogen gradient scaling, whereby the gradient automatically adjusts to variations in the size of tissue [3, 4].

Recently, there has been growing interest in an alternative mechanism for delivering morphogens to embryonic cells that employs so-called *cytonemes* [19, 20]. Cytonemes are thin, dynamic cellular extensions with a diameter of around 100 nm and lengths that vary from 1 to 100 μm, see Fig. 2. Although these filaments are observed in multiple biological systems, their precise function is still controversial. Nevertheless, cytonemes are actin-rich structures that can extend and retract relatively fast, and their tips have been seen to attach to other cells. It has thus been suggested that morphogens can be actively transported between source and target cells along actin filaments within a cytoneme via the action of myosin motors. One potential advantage of this active transport mechanism is that it provides an adaptable and precise form of cellular communication. Cytonemes have been most extensively characterized in the wing imaginal disc of *Drosophila* and have been associated with the transport of both morphogenetic protein Decapentaplegic (Dpp) and Hedgehog (Hg) [28, 7, 18, 29, 14, 10]. *Drosophila* cytonemes either emanate from the receptor-bearing target cells, transporting their receptors to the vicinity of source cells, or extend from the morphogen-producing cells, transporting morphogens to target cells. Increasing experimental evidence indicates that cytonemes also mediate morphogen transport in vertebrates [16, 31]. Examples include sonic hedgehog (Shh) cell-to-cell signaling in chicken limb buds [30] and Wnt signaling in zebrafish [33].

In contrast to diffusion-based mechanisms, there has been almost no mathematical modeling of cytoneme-based morphogenesis. One notable exception is a compartmental model due to Teimouri and Kolomeisky [34, 35]. These authors consider a discrete set of $N+1$ cells arranged on a line. A source cell at one end makes direct contact with each of the N target cells via a single cytoneme per cell. Assuming that the rate w_n of morphogen transport decreases with distance L_n between target and source cells, they show how a steady-state morphogen gradient can be established. Their model suggests that the direct delivery mechanism may be more robust than diffusion, but comes at an energy cost.

In this paper, we extend the model of Teimouri and Kolomeisky [34] by explicitly modeling the transport of morphogens along actin filaments. More specifically, we consider a simple bidirectional motor transport model, in which active particles carrying morphogens randomly switch between anterograde and retrograde transport. A crucial aspect of our model is the choice of boundary conditions at the source and target ends of each cytoneme. We take particles to be injected at a rate that is proportional to the particle concentration in the source cell, whereas we impose an absorbing boundary condition at the target end. A number of different features of our model are explored. First, we obtain an analytical steady-state solution of the transport equations, which enables us to identify the phenomenological rate w_n of

Ref. [34] with a biophysically derived expression. Interestingly, the energy cost in our model arises from the presence of retrograde transport. Second, we calculate the analog of the accumulation time considered in diffusion-based mechanisms [5, 6, 17]. This is important in order to check that the time to establish a morphogen gradient is consistent with developmental stages. Finally, we investigate the robustness of the model to fluctuations in the rate of morphogen production in the source cell.

2. Deterministic compartmental model

We begin by briefly reviewing the deterministic model of Ref. [34, 35]. Consider $N+1$ embryo cells arranged in a line, and introduce the cell label $n = 0, 1, \ldots, N$, see Fig. 3. Suppose that the cell $n = 0$ acts as the source cell and produces morphogens at a rate Q. (In anticipation of the motor-transport flux model, we will take a single particle to be a packet of signaling molecules that can be packed into a vesicle). The source cell also projects N tubular cytonemes, each of which attaches to a unique downstream cell. For simplicity, multiple contacts between the source cell and another cell are ignored so that each cytoneme inherits the label n of its target cell, $n = 1, \ldots, N$. Morphogens are transported to the nth target cell via the nth cytoneme at an n-dependent rate w_n, $n = 1, \ldots, N$. One interpretation of $1/w_n$ is the mean arrival time of signaling molecules to reach the target cell, assuming that this process has reached a stationary state. Finally, once morphogens have been delivered to a cell, they degrade at a rate k.

Let $P_n(t)$ denote the density of signaling molecules at the nth cell at time t. The corresponding evolution equations take the form [34]

$$\frac{dP_0}{dt} = Q - \sum_{n=1}^{N} w_n P_0(t), \tag{2.1a}$$
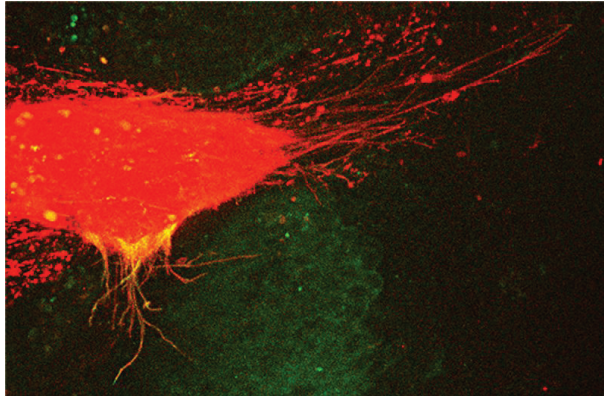
Figure 2. Micrograph showing cytonemes extending from tracheal cells of a *Drosophila* larva, which are marked with membrane-tethered mCherry fluorescent protein. Some of the cytonemes contact the underlying wing imaginal disc and transport the Dpp morphogen protein (marked with Green Fluorescent Protein) to the tracheal cells. [Creative commons figure originally generated by Thomas Korenberg.]
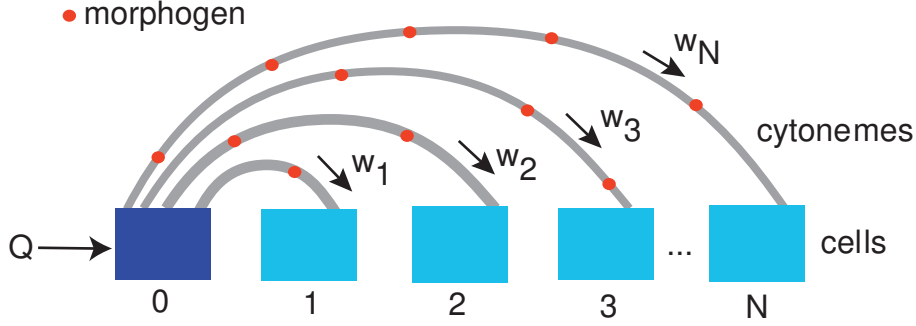
Figure 3. Schematic diagram of the cytoneme-based transport model introduced in Ref. [34]. A source cell (dark blue) generates morphogens at a rate Q, which are then delivered to other cells (light blue) via a set of tubular cytonemes. It is assumed that a single cytoneme links the source cell (labeled $n = 0$) to each target cell (labeled $n = 1, \ldots, N$), and transports morphogens (red dots) at a rate w_n.

$$\frac{dP_n}{dt} = w_n P_0(t) - k P_n(t), \quad n = 1, \ldots, N. \tag{2.1b}$$

Given the initial conditions $P_n(0) = 0$ for all n, these equations have the solution

$$P_0(t) = \frac{Q}{\eta} \left[1 - e^{-\eta t}\right], \tag{2.2a}$$

$$P_n(t) = \left[\frac{Q w_n}{\eta(\eta - k)}\right] e^{-\eta t} - \left[\frac{Q w_n}{k(\eta - k)}\right] e^{-kt} + \frac{Q w_n}{\eta k}, \tag{2.2b}$$

for $n = 1, \ldots, N$, where $\eta = \sum_{n=1}^{N} w_n$ and $\eta \neq k$. It follows that the stationary solution ($t \to \infty$) is

$$P_n^* = \frac{Q}{k\eta} w_n, \quad P_0^* = \frac{Q}{\eta}, \tag{2.3}$$

In order to determine a spatial morphogen gradient, it is necessary to specify the length L_n of the nth cytoneme and how w_n depends on L_n. Two formulations are considered in Ref. [34]. The first uses a statistical mechanical argument, whereby the rate of transport along a cytoneme is determined by the free-energy difference $\Delta G(n)$ arising from a morphogen being displaced from the source cell to the target cells:

$$w_n = W e^{-\Delta G(n)/k_B T},$$

where W is the background rate when $\Delta G(n) = 0$. Furthermore, the cytoneme length is taken to be $L_n = An$ and it is assumed that an amount of energy $\epsilon k_B T$ is spent in transferring a signaling molecule a distance l (presumably by active motor-driven transport). Hence,

$$\Delta G(n) = \frac{L_n}{l} \epsilon k_B T = \frac{n k_B T}{\xi}, \quad \xi = l/A\epsilon.$$

Finally, from equation (2.3) we have the stationary solution profile

$$P_n^* = \frac{QW}{k\eta} e^{-n/\xi}, \quad \eta = \frac{e^{-1/\xi} - e^{-(1+N)/\xi}}{1 - e^{-1/\xi}}. \tag{2.4}$$

This model thus predicts that the stationary distribution decays exponentially with spatial variable n, and the length constant ξ is larger when the transport is more efficient (smaller ϵ). The second model formulation treats each cytoneme as a one-dimensional lattice and consider transport of morphogens as a totally asymmetric exclusion process (TASEP), and identifies w_n with the stationary particle flux through the cytoneme to the nth target, see [34] for more details.

One of the potential limitations of the above model is that it ignores the dynamics of the transport process along the cytonemes, in the sense that w_n is determined from a stationary process. However, since the flux through the cytoneme couples to the dynamically varying concentration $P_0(t)$, we expect w_n also to be time-dependent. Although this would not affect the stationary-state, it could influence the approach to stationarity.

3. Bidirectional transport model

Consider a single cytoneme of length L linking a source cell to a single target cell, see Fig. 4. We now explicitly model the transport of morphogen containing vesicles by treating the cytoneme as a one-dimensional domain of length L and denote the density of motor-cargo complexes at $x \in [0, L]$ along the cytoneme by $u(x, t)$. We assume that the complexes can be partitioned into anterograde $(+)$ and retrograde $(-)$ subpopulations labeled by $u_+(x, t)$ and $u_-(x, t)$, respectively. (In the case of myosin transport along actin filaments, the retrograde flow would be due to treadmilling [39, 25]. For recent evidence of mysosin motor-based transport of puncta along cytonemes within the *Drosophila* wing imaginal disc, see [14]).) The corresponding differential Chapman-Kolmogorov equation takes the form

$$\frac{\partial u_+}{\partial t} = -v_+ \frac{\partial u_+}{\partial x} + \alpha u_- - \beta u_+ \tag{3.1a}$$

$$\frac{\partial u_-}{\partial t} = v_- \frac{\partial u_-}{\partial x} - \alpha u_- + \beta u_+, \tag{3.1b}$$

where $v_\pm$ are the speeds of the $\pm$ states, α is the rate of switching from the retrograde to the anterograde state, and β is the switching rate from anterograde to retrograde.
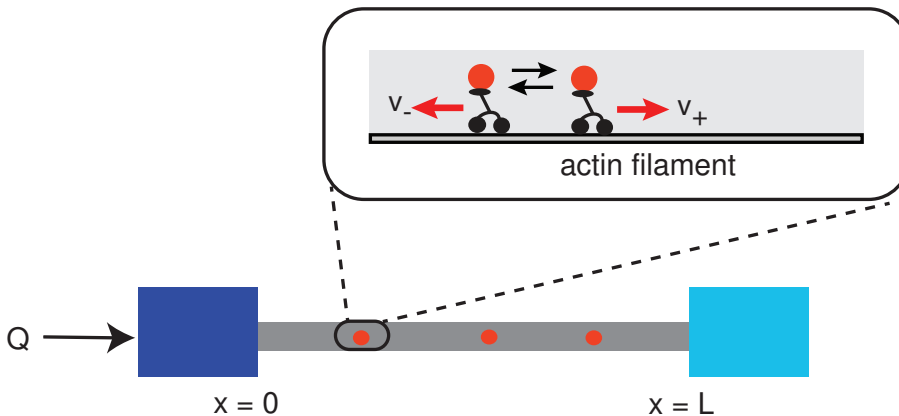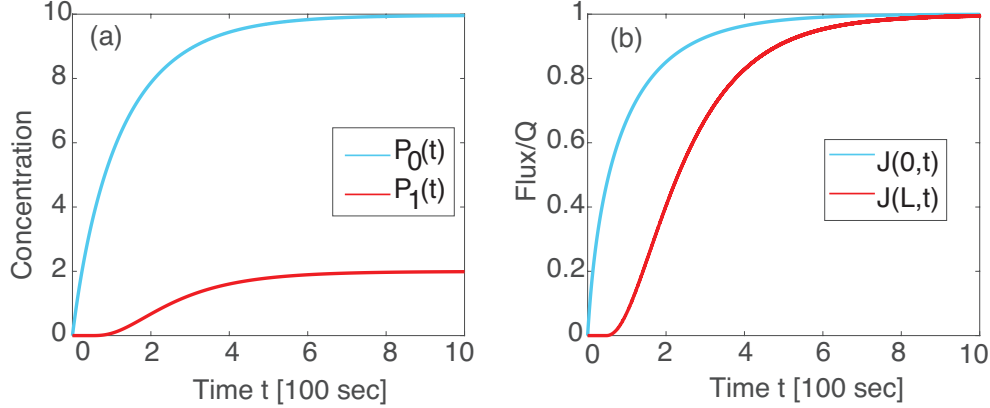

Figure 4. Bidirectional transport model of a single cytoneme.

Figure 5. Numerical solutions of the transport model for s single cytoneme. (a) Plots of morphogen concentrations $P_0(t), P_1(t)$ in the source and target cells as a function of time. (b) Corresponding plots of fluxes $J(0,t)$ and $J(L,t)$ at the two ends of the cytoneme. Morphogen is generated in source cell, $P_0(t)$, enters into cytoneme. Parameter values are as follows: $v_+ = 0.2\mu m\ s^{-1}$, $v_- = 0.1\mu m\ s^{-1}$, $\alpha = 0.1\ s^{-1}$, $\beta = 0.1\ s^{-1}$, $Q = 0.1\ s^{-1}$, $\kappa = 0.01\ s^{-1}$, $k = 0.05\ s^{-1}$, $L = 10\ \mu$ m s^{-1}. It follows that $\gamma = -0.5\mu m^{-1}$.

Equations (3.1a) and (3.1b) are supplemented by the boundary conditions

$$u_+(0,t) = \kappa P_0(t), \quad u_-(L,t) = 0, \tag{3.2}$$

where $P_0(t)$ is the density of vesicles in the source cell and κ is an injection rate. We assume that initially there are no particles within the cytonemes so $u_\pm(x,0) = 0$ for all $0 \le x \le L$. The transport component of the model couples to the number of vesicles in the source and target cells according to

$$\frac{dP_0}{dt} = Q - J(0,t), \quad \frac{dP_1}{dt} = J(L,t) - kP_1(t), \tag{3.3}$$

where Q is the particle production rate in the source cell and $J(x,t)$ is particle flux at position x at time t,

$$J(x,t) = v_+ u_+(x,t) - v_- u_-(x,t). \tag{3.4}$$

Example numerical solutions of the full system of equations are shown in Fig. 5. It can be seen that the morphogen concentrations in the source and target cells aproach steady-state values as $t \to \infty$. (In all figures we take the concentration to be dimensionless by defining a baseline concentration $P_{\text{base}} := Q/\alpha$ and setting $P_{\text{base}} = 1$.)

3.1. Stationary solution

We now calculate the steady-state solution P_0^*, P_1^* as a function of cytoneme length. Setting time derivatives to zero and adding equations (3.1a) and (3.1b) gives

$$\frac{d}{dx}\left(v_+ u_+(x) - v_- u_-(x)\right) = 0.$$
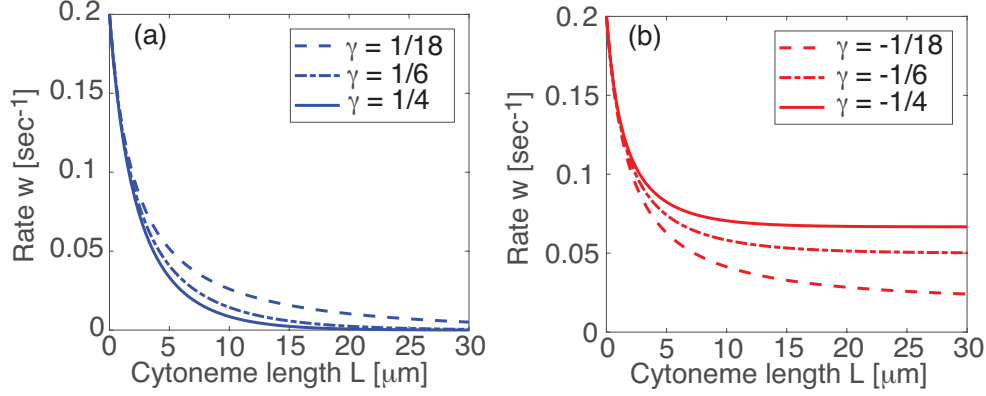
Figure 6. Transport rate $w(L)$ plotted as a function of cytoneme length L. (a) $\gamma > 0$ so that $\overline{v} < 0$ and the flux decays asymptotically to zero. (b) $\gamma < 0$ so that $\overline{v} > 0$ and the asymptote is non-zero. Same parameter values as Fig. 5 except for v_- and hence γ. (Units of γ are μm^{-1}.)

It follows that there is a stationary flux $J(x) = J_0$. Setting $dP_n/dt = 0$ in equation (3.3) implies that $J_0 = J(0) = Q$ and $P_1^* = Q/k$. Using these results to eliminate u_- from equation (3.1a), we have

$$\frac{du_+}{dx} + \gamma u_+ = -\frac{\alpha Q}{v_+ v_-}, \quad \gamma = \frac{\beta v_- - \alpha v_+}{v_+ v_-}$$

This has the solution (after imposing the boundary condition at $x = 0$)

$$u_+(x) = \kappa P_0^* e^{-\gamma x} - \frac{\alpha Q}{\gamma v_+ v_-} \left[1 - e^{-\gamma x} \right]. \tag{3.5}$$

(In the non-generic case that $\gamma = 0$, the concentration decreases linearly with x.) Finally, imposing the absorbing boundary condition at $x = L$, we can determine P_0^*. We thus obtain the results

$$P_0^* = \frac{Q}{w(L)}, \quad P_1^* = \frac{Q}{k}, \tag{3.6}$$

where

$$w(L) = \frac{\kappa v_+ e^{-\gamma L}}{1 + \alpha \left[1 - e^{-\gamma L}\right]/\gamma v_-}. \tag{3.7}$$

Note that $w(L) > 0$, since $e^{-\gamma L} - 1$ has the same sign as γ. An important quantity, which generalizes to the multi-cell case, is the ratio of the target and source densities,

$$\frac{P_1^*}{P_0^*} = \frac{w(L)}{k}. \tag{3.8}$$

The length-dependence of this ratio is determined by the function $w(L)$, which we identify as an effective cytoneme "conductance."

Two results follow from this. First, from (3.7), bidirectional transport can lead to a stationary flux that is an exponentially decaying function of cytoneme length provided that

$$\overline{v} = \frac{\alpha v_+ - \beta v_-}{\alpha + \beta} < 0, \quad \frac{\alpha}{\gamma v_-} \ll 1 \tag{3.9}$$

where $\bar{v}$ is the mean velocity of a motor-cargo complex. That is, in our dynamical transport model, spending sufficient time in the retrograde state effectively provides a free energy cost for transporting morphogens from the source cell to the target cell. Second, the asymptotic value $\lim_{L\to\infty} w(L)$ depends on the sign of $\bar{v}$, see Fig. 6. If $\bar{v} < 0$, then $w(L)$ decays to zero as cytoneme length tends to infinity. On the other hand, if $\bar{v} > 0$, then the anterograde transport state is dominant and one finds that

$$\lim_{L\to\infty} w(L) = \kappa v_+ \left(1 - \frac{\beta v_-}{\alpha v_+}\right), \tag{3.10}$$

Interestingly, a recent study of cytonmeme-based transport in the wing imaginal disc of *Drosophila* provides evidence for a significant retrograde component of motor-based transport [14]. They observed puncta moving at similar anterograde and retrograde speeds of around $0.4\mu m/s$. This does not necessarily imply that $\gamma = 0$, since the switching rates α and β could differ. Thus, rather than taking $v_- < v_+$ and $\alpha = \beta$, we could obtain a non-zero γ by taking $v_+ = v_-$ and $\alpha \neq \beta$. In ref. [14], periods between switching had an upper bound of $40s$, which implies that $\alpha, \beta > 0.02 s^{-1}$. (It would be straightforward to modify our choice of units so that our chosen parameters are comparable to Ref. [14], namely by taking the unit of time to be 10 seconds rather than 1 second. This would not affect any of our conclusions.)

3.2. Multiple target cells

One can extend the single cytoneme model to multiple cytonemes of length L_n linking a source cell to multiple target cells, $n = 1, \ldots, N$. We now have to specify the relative probability f_n that a morphogen is injected into the nth cytoneme, see Fig. 7. Let $u_+^n(x,t)$ and $u_-^n(x,t)$ be anterograde and retrograde subpopulations in the cytoneme contacting the n-th target cell. Then the bidirectional model for $u_\pm^n$ takes the same form as equations (3.1a) and (3.1b) on $x \in (0, L_n)$,

$$\frac{\partial u_+^n}{\partial t} = -v_+ \frac{\partial u_+^n}{\partial x} + \alpha u_-^n - \beta u_+^n \tag{3.11a}$$

$$\frac{\partial u_-^n}{\partial t} = v_- \frac{\partial u_-^n}{\partial x} - \alpha u_-^n + \beta u_+^n, \tag{3.11b}$$

with the modified boundary conditions

$$u_+^n(0,t) = \kappa f_n P_0(t), \quad u_-^n(L_n, t) = 0. \tag{3.12}$$

Extending (3.3) to the case of multiple target cells yields

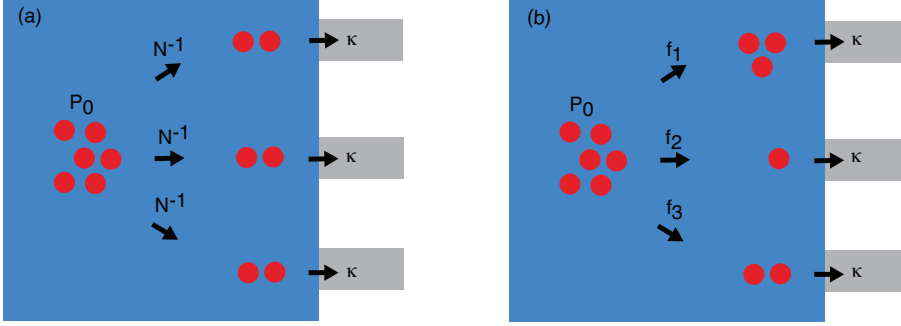$$\frac{dP_0}{dt} = Q - \sum_{m=1}^{N} J_m(0,t), \quad \frac{dP_n}{dt} = J_n(L_n, t) - kP_n \tag{3.13}$$

where

$$J_n(x,t) = v_+ u_+^n(x,t) - v_- u_-^n(x,t).$$

Solving the steady-state equations shows that

$$v_+ u_+^n(x) - v_- u_-^n(x) = J_n^*, \tag{3.14}$$

where J_n^* is the stationary flux reaching the n-th target cell, and

$$u_+^n(x) = \kappa f_n P_0^* e^{-\gamma x} - \frac{\alpha J_n^*}{\gamma v_+ v_-} \left[1 - e^{-\gamma x}\right]. \tag{3.15}$$

Figure 7. Allocation of resources in a source cell. (a) Uniform distribution of morphogens across $N = 3$ cytonemes. (b) Nonuniform distribution of morphogens across $N = 3$ cytonemes.

Imposing the absorbing boundary condition at $x = L_n$ implies that $J_n^* = f_n P_0^* w(L_n)$, with $w(L)$ given by equation (3.7). Finally, the stationary versions of equations (3.12) show that

$$P_0^* = \frac{Q}{\sum_{m=1}^{N} w_m}, \quad P_n^* = \frac{Q}{k} \frac{w_n}{\sum_{m=1}^{N} w_m} = \frac{w_n}{k} P_0^*, \tag{3.16}$$

where $w_n = f_n w(L_n)$. We thus recover the stationary solution of the compartmental model given by equations (2.3), except now w_n is derived explicitly from our transport model. It should also be noted that one cannot identify the time-dependent equations (3.13) with (3.3), since the flux rate $w_n P_0(t) \neq J_n(L_n, t)$ for finite t.

For the sake of illustration, we take $f_n = f(L_n)$ and consider three different choices for f: the uniform distribution

$$f_U(L_n) = 1/N, \tag{3.17}$$
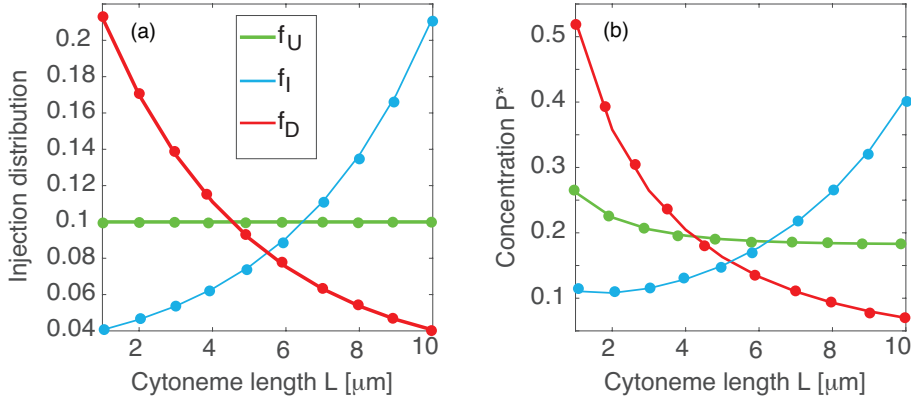
Figure 8. Steady-state morphogen gradients for various choices of injection distribution $f_n = f(L_n)$ with $N = 10$ and $L_n = n$. (a) Three different injection distributions: a uniform distribution f_U, a monotone increasing distribution f_I and a monotone decreasing distribution f_D. (b) Corresponding steady-state morphogen gradients $P_n^* = P^*(L_n)$. Other parameter values are as Fig. 5.

and the monotone increasing/decreasing distributions

$$f_I(L_n) = \frac{1}{\mathcal{N}_1}\left[e^{(L_n - L_1)/4} + 1\right], \quad f_D(L_n) = \frac{1}{\mathcal{N}_2}\left[e^{(L_N - L_n)} + 1\right], (3.18)$$

where $\mathcal{N}_1$ and $\mathcal{N}_2$ are normalization constants such that $\sum_{n=1}^{N} f(L_n) = 1$. Since each distribution can be re-expressed as a function of cytoneme length, $f_n = f(L_n)$, it follows that we can use equation (3.16) to determine the steady-state morphogen concentration $P_n^* = P^*(L_n)$. The results are shown in Fig. 8. Note, in particular, that allocating resources to longer cytonemes can actually reverse the gradient so that the concentration increases with distance of a target cell from the source cell. This suggests that one possible advantage of cytoneme-based rather than diffusion-based morphogen gradient formation is that the former has an additional mechanism of regulatory control, namely, determining how morphogenic resources are allocated to the various cytonemes projecting from a source cell. We model this in terms of a nonuniform injection probability distribution f_n. One physical mechanism underlying a non-uniform distribution could be variations in the number of cytonemes per target cell.

4. Properties of cytoneme-based morphogen gradient

4.1. Accumulation time

So far we have only considered the steady-state solution of the cytoneme-based model of morphogen gradient formation. As in the case of diffusion-based models, it is also important to consider the dynamics of gradient formation. In particular, we need to address the question of whether or not the time to form the morphogen gradient is small compared to the time of cell differentiation. The latter process involves surface receptors measuring the local value of the extracellular morphogen concentration and translating this information into a corresponding change in the activation of its signaling pathways and gene expression. If gradient formation is relatively fast, then cell fate is determined by the steady-state value of the local morphogen concentration, otherwise the cell has to interpret a time-varying morphogen concentration.

   In order to characterize the time-dependent approach to steady-state, we follow recent studies of diffusion-based models by considering the accumulation time [5, 6, 17] . First, we introduce the function

$$R_n(t) = 1 - \frac{P_n(t)}{P_n^*},$$

which represents the fractional deviation of the concentration from the steady-state P_n^*. Assuming that $R_n(t)$ is smooth enough and $P_n(0) = 0$, then $1 - R_n(t)$ is the fraction of the steady-state concentration that has accumulated by time t. The accumulation time is then defined by analogy with mean first passage times. That is, we average the time with respect to the accumulation time density according to

$$\tau_n = \int_0^\infty t \frac{\partial}{\partial t}\left(1 - R_n(t)\right) dt = \int_0^\infty R_n(t)dt. \tag{4.1}$$

The accumulation time can be calculated using Laplace transforms. That is, defining

$$\widehat{R}_n(s) = \int_0^\infty R_n(t)e^{-st}dt,$$

we have $\tau_n = \lim_{s\to 0} \widehat{R}(s)$. Integration by parts proves that $\lim_{s\to 0} s\widehat{P}_n(s) = P_n^*$. Hence,

$$\tau_n = \lim_{s\to 0} \frac{1}{s}\left(1 - \frac{s\widehat{P}_n(s)}{P_n^*}\right) = -\frac{1}{P_n^*}\frac{d}{ds}\, s\widehat{P}_n(s)\Big|_{s=0}. \tag{4.2}$$

The next step is to evaluate $\widehat{P}_n(s)$. Taking Laplace transforms of the second equation in (3.13) yields

$$s\widehat{P}_n(s) = \frac{v_+}{s+k}\cdot s\widehat{u}_+^n(L_n, s),$$

where we have used the initial condition $u_\pm^n(L, 0) = 0$. Substituting this and equation (3.16) into (4.2) and using

$$\lim_{s\to 0} s\widehat{u}_+^n(L_n, s) = u_+(L_n, \infty) = \frac{1}{v_+}J_n(L_n, \infty) = \frac{k}{v_+}P_n^*,$$

we have

$$\tau_n = \frac{1}{k} - \frac{v_+\sum_m w_m}{Qw_n}\frac{d}{ds}\, s\widehat{u}_+^n(L_n, s)\Big|_{s=0} \tag{4.3}$$

Now we want to find $\widehat{u}_+^n(x, s)$. Introduce the operators $\mathbb{L}_+ = \frac{1}{\alpha}(\partial_t + v_+\partial_x + \beta)$, $\mathbb{L}_- = \frac{1}{\beta}(\partial_t - v_-\partial_x + \alpha)u_-$ and $\mathbb{L} = \mathbb{L}_-\mathbb{L}_+$. We can then rewrite equations (3.1a) and (3.1b) for $u_\pm^n$ on $x \in [0, L_n]$ as

$$\mathbb{L}_+ u_+^n = u_-^n, \quad \mathbb{L}_- u_-^n = u_+^n \tag{4.4}$$

Since $\mathbb{L}_+$ and $\mathbb{L}_-$ commute, it follows that $\mathbb{L}u_\pm^n = u_\pm^n$, which is a version of the Telegrapher's equation. Imposing the initial conditions $u_\pm^n(x, 0) = 0$ for $x \in [0, L_n]$, and taking Laplace transforms yields

$$\partial_x^2\widehat{u}_\pm^n(x, s) - 2\left(s\delta - \frac{\gamma}{2}\right)\partial_x\widehat{u}_\pm^n(x, s) - \frac{s(s + \alpha + \beta)}{v_+v_-}\widehat{u}_\pm^n(x, s) = 0,$$

where $2\delta = 1/v_- - 1/v_+$. The corresponding general solution is given by

$$\widehat{u}_\pm^n(x, s) = \left[A_\pm^n(s)e^{f(s)x} + B_\pm^n(s)e^{-f(s)x}\right]e^{(s\delta - \gamma/2)x} \tag{4.5}$$

where the coefficients $A(s), B(s)$ are determined by the corresponding boundary conditions (3.12), and

$$4f^2(s) = \left(\frac{1}{v_+} + \frac{1}{v_-}\right)^2 s^2 + 2\left(\frac{1}{v_+} + \frac{1}{v_-}\right)\left(\frac{\beta}{v_+} + \frac{\alpha}{v_-}\right)s + \gamma^2.$$

Taking the time derivative of the boundary condition at $x = 0$, we have

$$\partial_t u_+^n(0, t) = f_n\kappa\partial_t P_0(t) = f_n\kappa[Q - \sum_m(v_+u_+^m(0, t) - v_-u_-^m(0, t))].$$

Laplace transforming this equation then yields

$$\frac{s}{f_n\kappa}(A_+^n(s) + B_+^n(s)) + v_+\sum_{m=1}^N(A_+^m(s) + B_+^m(s)) = v_-\sum_{m=1}^N(A_-^m(s) + B_-^m(s)) + \frac{Q}{s}. \tag{4.6}$$

Similarly, Laplace transforming the remaining boundary condition at $x = L_n$ gives

$$A_-^n(s)e^{L_nf(s)} + B_-^n(s)e^{-L_nf(s)} = 0. \tag{4.7}$$

We still need to generate two more equations for the four unknown coefficients $A_\pm^n(s)$ and $B_\pm^n(s)$ for fixed s and n. This can be achieved by Laplace transforming the first equation of (4.4),

$$(s + v_+ \partial_x + \beta)\widehat{u}_+^n(x, s) = \alpha \widehat{u}_-^n(x, s),$$

substituting for $\widehat{u}_\pm^n$ using (4.5), and comparing coefficients. We thus find that

$$g(s)A_+^n(s) = \alpha A_-^n(s), \quad h(s)B_+^n(s) = \alpha B_-^n(s), \tag{4.8}$$

where

$$g(s) = (1 + v_+\delta)s + \left(\beta - \frac{v_+\gamma}{2}\right) + v_+ f(s),$$
$$h(s) = (1 + v_+\delta)s + \left(\beta - \frac{v_+\gamma}{2}\right) - v_+ f(s).$$

Substituting equations (4.7) and (4.8) into (4.6) generates the following equation for the coefficients A_+^n:

$$s\left(h(s) - g(s)e^{2L_n f(s)}\right) A_+^n = \frac{\kappa f_n Q h(s)}{s} + \kappa f_n (v_+ - v_- h(s)/\alpha)g(s) \sum_{m=1}^{N} A_+^m e^{2L_m f(s)}$$

$$- \kappa f_n (v_+ - v_- g(s)/\alpha)h(s) \sum_{m=1}^{N} A_+^m.$$

Rearranging we have

$$A_+^n = \frac{\kappa f_n G(s)}{s a_n(s)} e^{-L_n f(s)}, \tag{4.9}$$

with

$$a_n(s) = h(s)e^{-L_n f(s)} - g(s)e^{L_n f(s)}, \tag{4.10a}$$

$$G(s) = \frac{Q h(s)}{s} + (v_+ - v_- h(s)/\alpha)g(s)\mathcal{A}_1 - (v_+ - v_- g(s)/\alpha)h(s))\mathcal{A}_0 \tag{4.10b}$$

and

$$\mathcal{A}_0 = \sum_{m=1}^{N} A_+^m, \quad \mathcal{A}_1 = \sum_{m=1}^{N} A_+^m e^{2L_m f(s)}. \tag{4.10c}$$

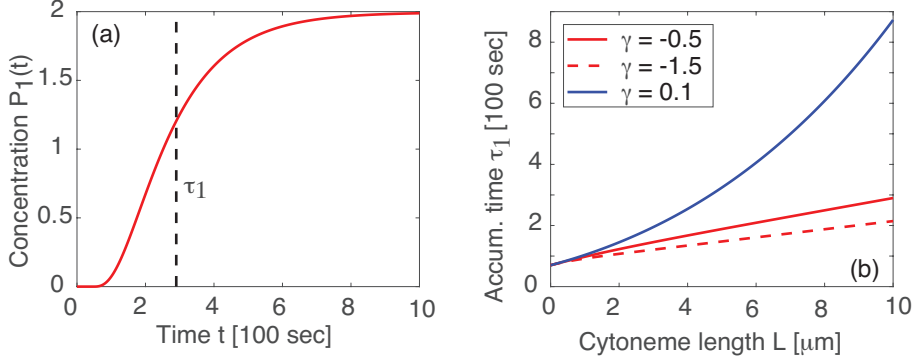Substituting equation (4.9) into equations (4.10c) shows that

$$\mathcal{A}_0 = \kappa G(s) \sum_{m=1}^{N} \frac{f_m}{a_m(s)} e^{-L_m f(s)}, \quad \mathcal{A}_1 = \kappa G(s) \sum_{m=1}^{N} \frac{f_m}{a_m(s)} e^{L_m f(s)} \tag{4.11}$$

Substituting these equations into (4.10b) and rearranging yields

$$G(s) = \frac{Q h(s)}{s q(s)} \tag{4.12}$$

with

$$q(s) = s + \kappa v_+ - \frac{\kappa v_-}{\alpha} g(s)h(s) \sum_{m=1}^{N} \left[e^{-L_m f(s)} - e^{L_m f(s)}\right] \frac{f_m}{a_m(s)}. \tag{4.13}$$

Figure 9. Accumulation time τ_1 for a single target cell. (a) Plot of the approach of $P_1(t)$ to the steady state P_1^* and the corresponding accumulation time τ_1. (b) Plot of the accumulation time as a function of cytoneme length for various values of γ. Other parameter values as Fig. 5.

Combining equations (4.7), (4.8), (4.9) and (4.12) gives

$$A_+^n(s) = h(s)e^{-L_n f(s)} \cdot \frac{\kappa Q}{s} \cdot \frac{f_n}{a_n(s)} \cdot \frac{1}{q(s)}$$

$$B_+^n(s) = -g(s)e^{L_n f(s)} \cdot \frac{\kappa Q}{s} \cdot \frac{f_n}{a_n(s)} \cdot \frac{1}{q(s)}.$$

and hence

$$s \cdot \widehat{u}_+^n(L_n, s) = -2v_+ \kappa Q f_n \cdot \frac{f(s)}{a_n(s)q(s)} \cdot e^{(\delta s - \gamma/2)L_n},$$

Substituting the above equation into (4.2) finally yields

$$\tau_n = \frac{1}{k} + 2\kappa v_+^2 \sum_{m=1}^{N} w_m \cdot e^{-\gamma L_n/2} \frac{f_n}{w_n} \cdot \frac{d}{ds} \left. \frac{e^{s\delta L_n} f(s)}{a_n(s)q(s)} \right|_{s=0}. \tag{4.14}$$

From equation (4.14), we can compute the accumulation time τ_n for the various injection distributions of equations (3.17) and (3.18). The results are depicted in Figs. 9 and 10. In order to set the baseline, we first consider a single cytoneme and target cell ($N = 1$) and plot the variation of accumulation time τ_1 with the cytoneme length $L_1 = L$, see Fig. 9. It can be seen that τ_1 is an increasing function of cytoneme length and also increases with γ. The latter means that increasing the level of retrograde flow increases the accumulation time. In the multi-cell case, we set $\tau_n = \tau_K(L_n)$ for $f_n = f_K(L_n)$, $K = U, I, D$, and plot the resulting accumulation times τ_K as a function of length, see Fig. 10(a). (In contrast to the single-cell model, the lengths of the cytonemes are fixed and $L = n$ identifies the length of the nth cytoneme.) One interesting result is that for each choice of injection distribution f_J there is crossover between the accumulation time curve $\tau_1(L)$ of a single target cell and the corresponding multi-cell accumulation time curve $\tau_K(L)$. This can be understood by taking a closer look at equation (4.14).

First, combining equations (3.13) and (4.1) shows that

$$\tau_n = \int_0^\infty \frac{t}{kP_n^*}[J_n(L_n, t) - \dot{P}_n]dt.$$
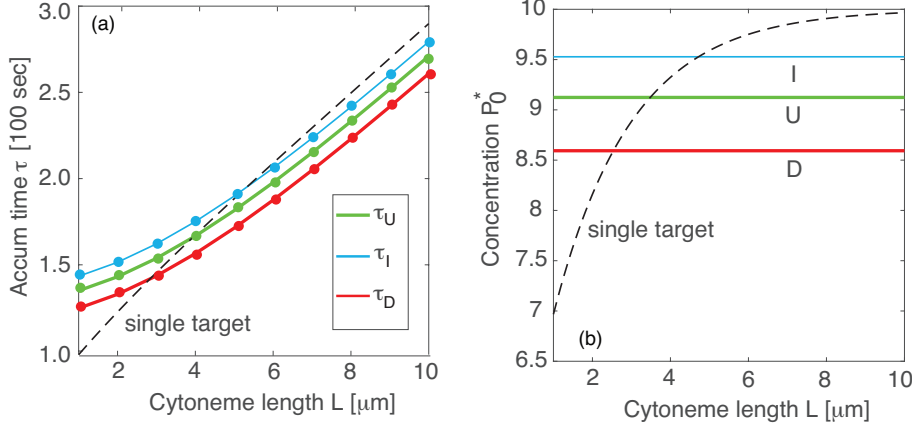
Figure 10. Accumulation times for multiple target cell model with $N = 10$ and $L_n = n$. (a) Accumulation time $\tau_K(L_n)$ for various injection distributions $f_K(L_n)$, $K = U, I, D$. Dashed curve shows corresponding accumulation time τ_1 for single target cell model where L now represents the length of a single cytoneme. (b) Steady-state concentration of source cell, P_0^*. In the case of a single target cell, P_0^* varies with respect to cytoneme length L. The corresponding steady-state concentrations for the three multi-cell cases $K = U, I, D$ are indicated by the horizontal lines. (Recall that the lengths of the cytonemes are fixed in the case of N target cells so P_0^*.) Other parameter values are as in Fig. 5.

Using the fact that $kP_n^* = J_n^*$, and performing an integration by parts gives

$$\tau_n = \frac{1}{k} + T_n(L_n), \tag{4.15}$$

where $T_n(x)$ is the accumulation time of $J_n(x, t)$,

$$T_n(x) = \int_0^\infty t \frac{\partial}{\partial t} \left(\frac{J_n(x, t)}{J_n^*} \right) dt. \tag{4.16}$$

Second, adding equations (3.11a) and (3.11b) and integrating with respect to x on $[0, L_n]$ yields

$$\frac{\partial}{\partial t} V_n(L_n, t) = J_n(0, t) - J_n(L_n, t), \tag{4.17}$$

where

$$V_n(L_n, t) = \int_0^{L_n} [u_+^n(x, t) + u_-^n(x, t)]dx.$$

Recall that the stationary flux at $x = 0$ and $x = L_n$ are the same. Hence, differentiating both sides of (4.17) with respect to t and multiplying by t/J_n^* gives

$$\frac{t}{J_n^*} \frac{\partial^2}{\partial t^2} V_n(L_n, t) = \frac{t}{J_n^*} \frac{\partial J_n(0, t)}{\partial t} - \frac{t}{J_n^*} \frac{\partial J_n(L_n, t)}{\partial t},$$

Performing an integration by parts then shows that

$$\int_0^\infty t \frac{\partial}{\partial t} \left(\frac{J_n(L_n, t)}{J_n^*} \right) dt = \int_0^\infty t \frac{\partial}{\partial t} \left(\frac{J_n(0, t)}{J_n^*} \right) dt + \frac{V_n(L_n, \infty)}{J_n^*},$$

that is,

$$T_n(L_n) = T_n(0) + \frac{V_n(L_n, \infty)}{J_n^*}. \tag{4.18}$$

From equations (4.15) and (4.18), one thus has

$$\tau_n = T_n(0) + \frac{V_n(L_n, \infty)}{J_n^*} + \frac{1}{k}. \tag{4.19}$$

It follows that the accumulation time of the n-th target cell is the sum of the accumulation time $T_n(0)$ of $J_n(0, t)$, and two terms that are independent of the number of cytonemes N. In order to establish that $V_n(L_n, \infty)/J_n^*$ is independent of N, we substitute for $u_-^n(x)$ using the steady-state flux condition (3.14) gives

$$V_n(L_n, \infty) = \int_0^{L_n} \left[\left(1 + \frac{v_+}{v_-}\right) u_+^n(x) - \frac{J_n^*}{v_-} \right] dx.$$

Now substituting for $u_+^n(x)$ using equation (3.15) yields

$$V_n(L_n, \infty) = \left(1 + \frac{v_+}{v_-}\right) \left(\kappa f_n P_0^* + \frac{\alpha J_n^*}{\gamma v_+ v_-}\right) \frac{1 - e^{-\gamma L_n}}{\gamma}$$
$$- L_n J_n^* \left(\left(1 + \frac{v_+}{v_-}\right) \frac{\alpha}{\gamma v_+ v_-} + \frac{1}{v_-} \right).$$

Dividing through by J_n^* and using equation (3.6), we have

$$\frac{V_n(L_n, \infty)}{J_n^*} = \left(1 + \frac{v_+}{v_-}\right) \left(\frac{\kappa}{w(L_n)} + \frac{\alpha}{\gamma v_+ v_-}\right) \frac{1 - e^{-\gamma L_n}}{\gamma}$$
$$- L_n \left(\left(1 + \frac{v_+}{v_-}\right) \frac{\alpha}{\gamma v_+ v_-} + \frac{1}{v_-} \right) := V(L_n). \tag{4.20}$$

This establishes that the contribution V_n/J_n^* is the same function of length for the single target cell and multiple cell cases. Thus, equation (4.19) implies that the difference between the accumulation time curve $\tau_1(L)$ of a single target cell and the corresponding accumulation time curve $\tau_K(L)$ of the multiple cell case arises from the term $T_n(0)$. Since $J_n(0, t) = v_+ \kappa P_0(t) - v_- u_-(0, t)$, it follows that $T_n(0)$ depends on the time to reach the steady-state concentration of the source cell, P_0^*. In particular, higher P_0^* implies larger $T_n(0)$. This suggests that the crossover in Fig. 10(a) can be understood by comparing the steady-state concentration P_0^* of the multi-cell model with P_0^* for a single cytoneme of length $L = n$, see Fig. 10(b).

4.2. Robustness of morphogen gradient

A major focus of research on morphogen gradients is the robustness of patterning based on morphogen gradient with respect to changes in environmental conditions such as the morphogen production rate Q [15]. Following previous studies of diffused-based morphogenesis, we will characterize the sensitivity of the cytoneme-based morphogen gradient to fluctuations in Q by considering the corresponding induced spatial shift in morphogen concentration. For analytical convenience, we replace the discrete set of target cells $n = 1, \ldots, N$ by a continuum of target cells distributed uniformly on the domain $y \in [0, \mathfrak{L}]$ such that $P_n(t) \to P(y, t)$ and $J_n(t) \to J(y, t)$. The source cell is treated as a single compartment with particle density $P_0(t)$. Equations (3.1a)

and (3.1b) still hold with $u_\pm^n(x,t) \to u_\pm(x,y,t)$, while the boundary conditions (3.2) become

$$u_+(0,y,t) = \kappa f(y)P_0(t), \quad u_-(L(y),t) = 0. \tag{4.21}$$

Here $L(y)$ is the length of cytonemes contacting cells at y and $f(y)$ is the probability density of particles being injected into these cytonemes such that

$$\int_0^{\mathfrak{L}} f(y)dy = 1.$$

Finally, the transport component of the model couples to the distributions of particles in the source and target cells according to

$$\frac{dP_0}{dt} = Q - \int_0^{\mathfrak{L}} J(0,y,t)dy, \quad \frac{\partial P(y,t)}{dt} = J(L(y),y,t) - kP(y,t), \tag{4.22}$$

where $J(x,y,t)$ is the particle flux at position x at time t through the cytonemes linking the source cell to cells at y:

$$J(x,y,t) = v_+ u_+(x,y,t) - v_- u_-(x,y,t). \tag{4.23}$$

We assume that both $f(y)$ and $L(y)$ are smooth functions of y. As a further simplification, we set $L(y) = y$ so $\mathfrak{L} = L$.

For fixed y, the steady-state solution of the transport equations (3.1a) and (3.1b) can be solved as before. We thus obtain the steady-state solutions

$$P_0^* = \frac{Q}{\int_0^L f(y)w(y)dy}, \quad P^*(y) = \frac{Q}{k} \cdot \frac{f(y)w(y)}{\int_0^L f(y)w(y)dy}. \tag{4.24}$$

Consider some threshold morphogen concentration P_c and denote the cellular position where this threshold occurs by y_c, that is,

$$P^*(y_c) = P_c. \tag{4.25}$$
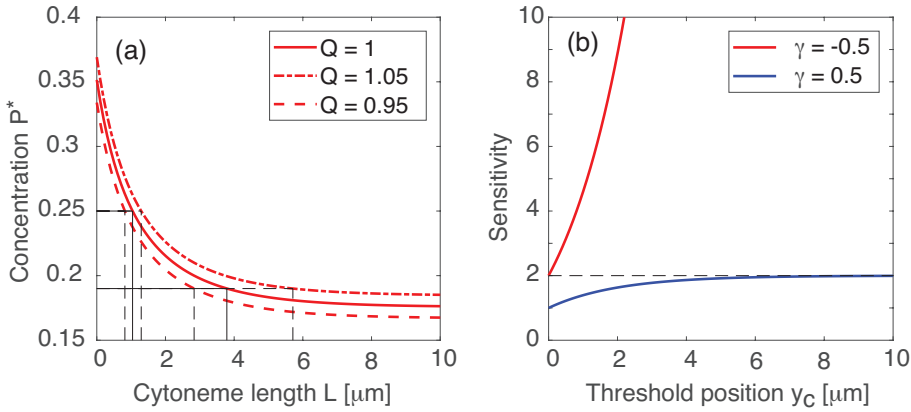
Figure 11. Sensitivity of the threshold position y_c with respect to fluctuations in Q in the case of a uniform injection probability density $f(y) = 1/L$. (a) A perturbation in Q also perturbs the threshold position y_c. (b) Plot of sensitivity dy/dQ as a function of the threshold position y_c. If $\gamma > 0$ then the sensitivity is bounded, wheres if $\gamma < 0$ then the sensitivity increases exponentially. Other parameters as in Fig. 5.

We wish to determine the shift in threshold position $y_c \to y_c + \Delta y_c$ in response to a shift in the production rate, $Q \to Q + \Delta Q$. Since $\Gamma := \int_0^L f(y)w(y)dy$ is fixed, we have

$$Qf(y)w(y) = (Q + \Delta Q)f(y + \Delta y)w(y + \Delta y)$$
$$= (Q + \Delta Q)f(y)w(y) + Q(f'(y)w(y) + f(y)w'(y))\Delta y.$$

Rearranging and taking the limits $\Delta Q, \Delta y \to 0$ yields the sensitivity

$$\left.\frac{dy}{dQ}\right|_{y=y_c} = -\frac{f(y_c)w(y_c)}{Q[f'(y_c)w(y_c) + f(y_c)w'(y_c)]}. \tag{4.26}$$

For example, assuming uniform injection probability $f(y) = 1/L$ gives

$$\left.\frac{dy}{dQ}\right|_{y=y_c} = -\frac{w(y_c)}{Qw'(y_c)} = \frac{1}{Q\gamma} \cdot \frac{v_- \gamma + \alpha(1 - e^{-\gamma y_c})}{v_- \gamma + \alpha}, \tag{4.27}$$

where we have used equation (3.7).

The sensitivity with respect to Q has different behavior depending on the sign of γ. This is illustrated in Fig. 11 for $f = f_U(y) = 1/L$. If $\gamma > 0$, so that the mean velocity of motor-cargo complex satisfies $\overline{v} < 0$, then $0 < e^{-\gamma y_c} \leq 1$. Hence,

$$0 < \left.\frac{dy}{dQ}\right|_{y=y_0} < \frac{1}{Q\gamma}, \tag{4.28}$$

and the sensitivity with respect to fluctuations in Q is bounded regardless of the size of y_c. On the other hand, if $\gamma < 0$ with $\overline{v} > 0$, then $e^{-\gamma y_c} \geq 1$. It follows that

$$\left.\frac{dy}{dQ}\right|_{y=y_0} = \frac{1}{Q|\gamma|}\left[\frac{1}{1 - |\gamma|v_-/\alpha}e^{|\gamma|y_c} - 1\right] > 0. \tag{4.29}$$

Therefore, the sensitivity is always positive and increases exponentially with respect to y_c. Our analysis strongly suggests that in order to ensure that the morphogen gradient is not exponentially sensitive to fluctuations in the production rate, it is necessary that $\overline{v} < 0$. This reinforces the observation of Ref. [34] that robustness comes at the expense of an energy cost, in this case a strong retrograde flow.

To see how robustness depends on the choice of the distribution $f(y)$ we consider continuum versions of equations (3.18),

$$f_I(y) = \frac{e^{y/4} + 1}{\mathcal{N}_3}, \quad f_D(y) = \frac{e^{(L-y)/4} + 1}{\mathcal{N}_4}, \tag{4.30}$$

where $\mathcal{N}_3$ and $\mathcal{N}_4$ are normalization constants such that $\int_0^L f(y)dy$. The resulting sensitivity curves are shown in Fig. 12.

5. Discussion

In this paper, we considered a simple bidirectional motor transport model for the flux of morphogens along a set of cytonemes, which link a source cell to a one-dimensional array of target cells. We obtained an analytical steady-state solution of the transport equations, which enabled us to identify the phenomenological transport rate of Ref. [34] with a biophysically derived expression. In particular, we related the energy cost of cytoneme-based morphogenesis with the degree of retrograde transport. We then investigated various properties of the resulting morphogen gradient, including its accumulation time, and its robustness to fluctuations in the rate of morphogen
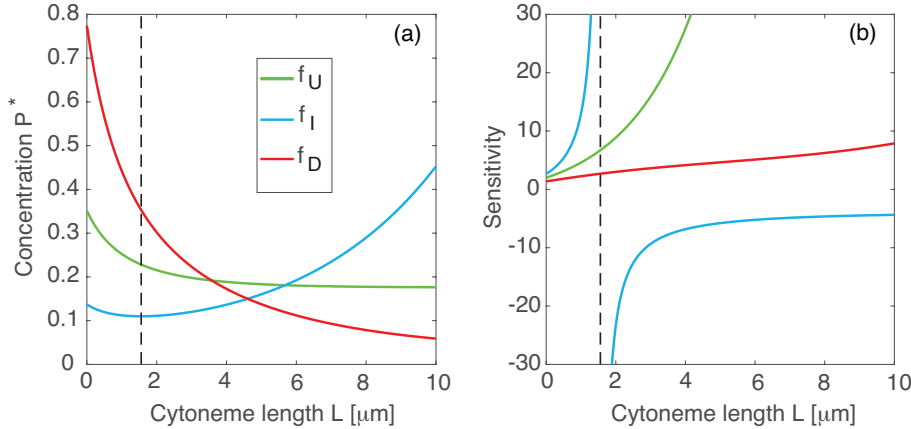
Figure 12. Sensitivity of the threshold position y_c with respect to fluctuations in Q in the case of different injection probability densities $f_K(y)$, $K = U, I, D$. (a) Unperturbed steady-state morphogen gradients. (b) Corresponding sensitivity curves. Other parameter values are as in Fig. 5.

production in the source cell. One important parameter that emerged from our analysis is

$$\gamma = \frac{\beta v_- - \alpha v_+}{v_+ v_-} = -\bar{v}\frac{\alpha + \beta}{v_+ v_-},$$

where $\bar{v}$ is the mean motor velocity, $v_\pm$ are the anterograde and retrograde speeds, and α, β are the velocity switching rates. First, the rate of decay of the morphogen gradient depends on $|\gamma|$. Second, the sign of γ determines the asymptotic behavior of the morphogen concentration for long cytonemes. We found that the asymptotic behavior was consistent with diffusion-based mechanisms if $\gamma > 0$, which implies that $\bar{v} < 0$ and retrograde flow dominates. More significantly, in order to obtain a bounded sensitivity to fluctuations in the morphogen production rate Q, it was necessary for $\gamma > 0$. A recent experimental study is at least consistent with the idea that there is significant retrograde flow [14]. Another finding of the latter study is that puncta along a cytoneme can undergo periods of stalling. It would be straightforward to add a stalled state into our transport model. However, it would not affect the main conclusion of our work.

Another interesting feature of our transport model, which is absent in diffusion-based models, is that morphogenic resources can be non-uniformly allocated to the various cytonemes projecting from a source cell, which could reflect variations in the number of cytonemes per target cell, for example. This competition for resources provides a potential substrate for regulatory control, which could lead to a variety of possible morphogen concentration profiles, including those that are non-monotonic.

One of the major simplifying assumptions of our cytoneme-based transport model is that each cytoneme projecting from a source cell is attached to its target cell for significant periods. However, it has been found experimentally that cytonemes do not remain permanently attached, undergoing alternating periods of retraction and growth [19, 14, 10]. This needn't be inconsistent with our model because all we require is that there is cytoneme-mediated contact between the source and target

cells for a sufficient time - presumably consistent with the accumulation time. Hence, this could be maintained by a population of cytonemes, whose individual members are dynamic. It should also be noted that there is evidence that cytonemes can be stabilized by their targets [10]. Nevertheless the dynamic nature of cytonemes raises two interesting issues that we hope to explore in future work. First, one could model dynamic interactions between the cytoneme tip and the target cell as a stochastic process, which then couples to the transport model as a switching boundary condition at the target end of the cytoneme. It should then be possible to analyze the resulting stochastic transport model along analogous lines to recent studies of advection-diffusion equations in domains with randomly switching boundaries [12, 13]. Second, cytonemes also need to find their target cells in the first place. It has been suggested that this could occur either via a random search process based on retraction and growth, or via some chemoattractant [19]. There are certain parallels with microtubules of the mitotic spindle searching for kinetochores prior to separation of cytochrome pairs [11], although it is important to note that cytonemes are actin-based. Finally, it would also be interesting to explore to what extent direct contacts via cytonemes play a role in other types of cellular self-organization that are traditionally based on diffusive transport, such as Turing pattern formation. This will also require understanding within the context of morphogenesis the interplay between cytonemes that transport receptors to source cells and those that transport ligands to target cells; we focused on the latter in this paper.

Acknowledgements

References

[1] Ashe H L and Briscoe J 2006 The interpretation of morphogen gradients. *Development* **133** 385–394.

[2] Barkai N and Shilo B Z 2009 Robust generation and decoding of morphogen gradients. *Cold Spring Harb. Perspect. Biol.* **1** a001362.

[3] Ben-Zvi D and Barkai N 2010 Scaling of morphogen gradients by an expansion-repression integral feedback control. *Proc. Natl. Acad. Sci. USA* **107** 6924–6929.

[4] Ben-Zvi D, Shilo B Z and Barkai N 2011 Scaling of morphogen gradients. *Curr. Opin. Genet. Dev.* **21** 704–710.

[5] Berezhkovskii A M, Sample C, Shvartsman S Y 2010 How long does it take to establish a morphogen gradient? Biophys J **99** L59-L61.

[6] Berezhkovskii A M, Sample C, Shvartsman S Y 2011 Formation of morphogen gradients: local accumulation time. *Phys Rev E* **83** 051906.

[7] Bischoff M, Gradilla A C, Seijo I, Andres G, Rodriguez-Navas C, Gonzalez-Mendez L and Guerrero I 2013 Cytonemes are required for the establishment of a normal Hedgehog morphogen gradient in Drosophila epithelia. *Nat Cell Biol* **15** 1269-1281

[8] Bollenbach T, Kruse K, Pantazis P, Gonzalez-Gaitan M and Julicher F 2005 Robust formation of morphogen gradients. *Phys. Rev. Lett.* **94** 018103.

[9] Bollenbach T, Pantazis P, Kicheva A, Bokel C, Gonzalez-Gaitan M and Julicher F 2008 Precision of the dpp gradient. *Development* **135** 1137–1146.

[10] Bodeen W J, Marada S, Truong A and Ogden S K 2017 A fixation method to preserve cultured cell cytonemes facilitates mechanistic interrogation of morphogen transport. *Development* **144** 3612-3624.

[11] Bressloff P C 2014 *Stochastic Processes in Cell Biology* Springer Berlin

[12] Bressloff P C and Lawley S D 2015 Moment equations for a piecewise deterministic PDE. *J. Phys. A* **48** 105001

[13] Bressloff P C and Lawley S D 2015 Escape from subcellular domains with randomly switching boundaries. *Multiscale Model. Simul.* **13** 1420-1455.

[14] Chen W, Huang H, Hatori R and Kornberg T B 2017 Essential basal cytonemes take up Hedgehog in the Drosophila wing imaginal disc. *Development* **144** 3134-3144.

[15] Eldar A, Rosin D, Shilo B Z and Barkai N 2003 Self-enhanced ligand degradation underlies robustness of morphogen gradients. *Dev. Cell* **5** 635–646.

[16] Fairchild C L and Barna M 2014 Specialized filopodia: at the tip of morphogen transport and vertebrate tissue patterning. *Curr. Opin. Genet. Dev.* **27** 67-73.

[17] Gordon P, Sample C, Berezhkovskii A M, Muratov C B and Shvartsman S Y 2011 Local kinetics of morphogen gradients. *Proc Natl Acad Sci* **108** 6157-6162.

[18] Gradilla A C and Guerrero I 2013 Cytoneme-mediated cell-to-cell signaling during development. *Cell Tissue Res.* **352** 59-66.

[19] Kornberg T B and Roy S 2014 Cytonemes as specialized signaling filopodia. *Development* **141** 729-736.

[20] Kornberg, T. B: Cytonemes and the dispersion of morphogens. WIREs Dev Biol 2014, 3:445-463

[21] Kruse K, Pantazis P, Bollenbach T, Julicher F and Gonzalez-Gaitan M 2004 Dpp gradient formation by dynamin-dependent endocytosis: receptor trafficking and the diffusion model. *Development* **131** 4843–4856.

[22] Lander A D 2011 Pattern, growth and control. *Cell* **144** 955–969.

[23] Lander A D, Lo W C, Nie Q and Wan F Y 2009 The measure of success: constraints, objectives, and tradeoffs in morphogen-mediated patterning. *Cold Spring Harb. Perspect. Biol.* **1** a002022.

[24] Lander A D, Lo W C and Wan F Y 2002 Do morphogen gradients arise by diffusion? *Dev. Cell.* **2** 785–796.

[25] Naoz M, Manor U, Sakaguchi H, Kachar B and Gov N S 2015 Protein localization by actin treadmilling and molecular motors regulates stereocilia shape and treadmilling rate *Biophys. J.* **95** 5706-5718

[26] Perez-Carrasco, R, Guerrero P, Briscoe J and Page K M 2016 Intrinsic noise profoundly alters the dynamics and steady state of morphogen controlled bistable genetic switches. *PLoS Comput Biol* **12** e1005154.

[27] Rorth P 2014 Reach out and touch someone. *Science* **343** 848-849.

[28] Roy S, Hsiung F and Kornberg T B 2011 Specificity of Drosophila cytonemes for distinct signaling pathways. *Science* **332** 354-358

[29] Roy S and Kornberg T 2015 Paracrine signaling mediated at cell- cell contacts. *BioEssays* **37** 25-33.

[30] Sanders T A, Llagostera E and Barna M 2013 Specialized filopodia direct long-range transport of SHH during vertebrate tissue patterning. *Nature* **497** 628-632.

[31] Sagar F P and Scaal M 2016 Signaling filopodia in vertebrate embryonic development. *Cell Mol Life Sci* **73** 961-974

[32] Shvartsman S Y and Baker R E 2012 Mathematical models of morphogen gradients and their effects on gene expression. *Rev. Dev Biol* **1** 715–730.

[33] Stanganello E and Scholpp S 2016 Role of cytonemes in Wnt transport. *J. Cell Sci.* **129** 665-672.

[34] Teimouri H and Kolomeisky A B 2016 New model for understanding mechanisms of biological signaling: direct transport via cytonemes. *J. Phys. Chem. Lett.* **7** 180-185.

[35] Teimouri H and Kolomeisky A B 2016 Mechanisms of the formation of biological signaling profiles. *J. Phys. A: Math. Theor.* **49** 483001.

[36] Wang Q, Holmes W R, Sosnik J, Schilling T and Nie Q 2017 Cell sorting and noise-induced cell plasticity coordinate to sharpen boundaries between gene expression domains. *PLoS Comp. Biol.* **13** e1005307.

[37] Wartlick O, Kicheva A and Gonzalez-Gaitan M 2009 Morphogen gradient formation. *Cold Spring Harb. Perspect. Biol.* **1** a001255.

[38] Wolpert L 1969 Positional information and the spatial pattern of cellular differentiation. *J. Theor. Biol.* **25** 1–47.

[39] Yochelis A, Ebrahim S, Millis B, Cui R, Kachar B, Naoz M and Gov N S 2015 Self-organization of waves and pulse trains by molecular motors in cellular protrusions *Scientific Reports* **5** 13521

[40] Zhang L, Radtke K, Zhengand L, Cai A Q, Schilling T F and Nie Q 2012 Noise drives sharpening of gene expression boundaries in the zebrafish hindbrain. *Mol. Syst. Biol.* **8** 613.